RSC Advances

PAPER

View Article Online
View Journal | View Issue

Cite this: *RSC Adv.*, 2019, **9**, 12339

Transport property of ligand-driven light-induced spin-change Fe-based spin crossover complexes†

Feifei Li,[a] Jing Huang,*[a] Yujie Hu[b] and Qunxiang Li *[bc]

The Fe-based spin-crossover (SCO) complexes, especially the ligand-driven light-induced spin-change (LD-LISC) systems with high spin-transition temperature, are considered as the most promising building blocks for designing molecular spintronic devices due to their bistability between the high-spin (HS) and low-spin (LS) states. Here, we explore the transport properties of $Fe(stpy)_4(NCS)_2$ LD-LISC SCO complexes with the *trans* and *cis* configurations sandwiched between Au electrodes by performing extensive density functional theory calculations combined with the non-equilibrium Green's function method. As for the *trans* configuration, the current through the molecular junction with the HS state is significantly larger than that of the LS state, which indicates that this Fe-based LD-LISC SCO complex with the *trans* configuration could act as a molecular switch when the spin transition is triggered by external stimuli. Remarkably, we observe the nearly perfect spin-filtering effect and obvious negative differential resistance feature in the $Fe(stpy)_4(NCX)_2$ junctions with the *trans* and *cis* configurations, which is attributed by the dramatically different electronic structures of two spin channels and the bias-dependent transmission spectra, respectively. These obtained theoretical findings suggest that the examined Fe-based LD-LISC SCO complexes hold great potential in molecular spintronics.

Received 25th February 2019
Accepted 15th April 2019

DOI: 10.1039/c9ra01420a

rsc.li/rsc-advances

1 Introduction

The most interesting and investigated feature of spin-crossover (SCO) complexes, formed by metal ions in surrounding ligands, is the transition between the low-spin (LS) (usually the ground state) and high-spin (HS) states of the central metal ion, which can be triggered by temperature, pressure, and light as well as electric and magnetic fields.[1–4] The switching between the LS and HS states has been observed in many SCO complexes of d^4–d^7 transition metal ions, but the Fe-based SCO complexes (d^6) account for more than 90% of known SCO materials.[5,6] Due to the different electronic configurations of the 3d electrons, these Fe-based complexes with the HS and LS states display the dramatically different optical, electronic, and magnetic properties, and they are considered as promising candidates for future applications, such as sensor, display, information storage and molecular spintronic devices. Therefore, more attention should be paid to the transport properties of these Fe-based SCO complexes.

In experiments, one of the possible mechanisms for the observed SCO behavior is the light-induced excited spin state trapping (LIESST) effect, which is encountered in many Fe-based SCO complexes. Nevertheless, until now their applications are prohibited since the lifetimes of the photomagnetic states are long enough only at low temperature.[7,8] In practical applications, the SCO complexes spin switch should ideally operate under atmospheric pressure and at room temperature. Fortunately, a family of SCO systems containing photoactive ligands, which can work at high temperature (*i.e.* up to room temperature), have been driven more attention in molecular spin switch.[9–11] These compounds always present the spin transition upon the conformational changes *via* the reversible *cis–trans* isomerization or ring-closing/ring-opening reactions under electromagnetic radiation, and then they exhibit the so-called ligand-driven light-induced spin-change (LD-LISC) effect. Many promising photoactive ligands in these LD-LISC systems including stilbene, azobenzene, diarylethene, and styrylpyridine, have been successfully synthesized.[12–15] Among the Fe-based LD-LISC SCO systems, the family of $Fe(stpy)_4(NCX)_2$ (X = S, Se, and BH_3, stpy = *cis*- or *trans*-styrylpyridine isomers) complexes is of particular interest.[16–20] They display different magnetic property depending on the stpy ligand, and the SCO temperature is up to about 300 K for X = BH_3.[21]

Previous experimental and theoretical investigations of Fe-based SCO complexes mainly focus on crystal structure, temperature-dependent effective magnetic moment, photocyclization, photoswitching, and so on.[1,2] The transport

[a]*School of Materials and Chemical Engineering, Anhui Jianzhu University, Hefei, Anhui 230601, China. E-mail: jhuang@ustc.edu.cn*

[b]*Hefei National Laboratory for Physical Sciences at the Microscale, University of Science and Technology of China, Hefei, Anhui 230026, China. E-mail: liqun@ustc.edu.cn*

[c]*Synergetic Innovation Center of Quantum Information and Quantum Physics, University of Science and Technology of China, Hefei, Anhui 230026, China*

† Electronic supplementary information (ESI) available. See DOI: 10.1039/c9ra01420a

behavior of Fe-based LD-LISC SCO complexes is limited so far, mostly because it is very challenging due to difficulties associated with the controllable anchoring contact in devices.[22,23] In this work, we explore the transport properties of $Fe(stpy)_4(NCS)_2$ SCO complexes with the *trans* and *cis* configurations sandwiched between two Au nanoelectrodes by performing extensive density functional theory calculations combined with non-equilibrium Green's function method. As for the *trans* configuration, the current through the molecular junction with the HS state is significantly larger than that of the LS state, which indicates that this Fe-based SCO complex with the *trans* configuration could act as a molecular switch when the spin transition is triggered by external stimuli. Moreover, we observe the nearly perfect spin-filtering effect and obvious negative differential resistance feature for $Fe(stpy)_4(NCX)_2$ with the *trans* and *cis* configurations, which is attributed by the remarkably different electronic structures of two spin channels and the bias-dependent transmission spectra, respectively. Moreover, the predicted energy barrier of the *trans*-LS → *cis*-HS spin transition is close to the energy of light radiation to realize the SCO phenomena in experiments.

2 Computational methods

Here, geometric optimizations, electronic structures, and SCO behaviors of $Fe(stpy)_4(NCS)_2$ complexes are carried out by using Gaussian package[24] at the *meta*-GGA hybrid TPSSh functional level since previous investigation has shown that the TPSSh functional can be capable of reproducing the correct ground state of the Fe containing complexes.[21] In our calculations, the fully optimized contracted triple-ξ with polarization functional Gaussian basis sets, developed by Ahlrichs and co-workers,[25] are employed for all elements, which could be capable of reproducing the electronic structure and energy difference in several spin-crossover systems.[26,27] Geometry optimizations are performed with a convergence criterion of 10^{-3} atomic unit (a.u.) on the gradient, 10^{-3} a.u. on the displacement, and 10^{-5} a.u. on the energy.

The transport behaviors of these proposed junctions are calculated by using the Atomistix ToolKit (ATK) package,[28,29] which combines density functional theory (DFT) with non-equilibrium Green's function method (see ESI†). The generalized gradient approximation in the Perdew–Burke–Ernzerhof form (GGA-PBE) is used to describe the exchange and correlation energy. The interaction between ionic cores and valence electrons is modeled with the Troullier–Martins nonlocal pseudopotential. Double-zeta plus polarized basis sets are chosen for all atoms. An energy cutoff is set to be 150 Ry for the real-space grid on which the Poisson equation is self-consistently solved. The spin-resolved transmission coefficients of these molecular junctions are calculated using

$$T_\sigma(E, V) = \mathrm{Tr}[\Gamma_L G_\sigma \Gamma_R G_\sigma^+], \quad (1)$$

where G_σ is the spin-dependent retarded Green's function of the extended molecule, $\Gamma_{L/R}$ is the coupling matrix between the extended molecule and the left/right electrode, and σ stands for the spin-up (↑) and spin-down (↓) channels. The current through the molecular junction is obtained by using the Landauer–Büttiker formula

$$I(V) = \frac{e}{h}\int T_\sigma(E, V)[f(E-\mu_L) - f(E-\mu_R)]\mathrm{d}E, \quad (2)$$

here, the $f(E-\mu)$ is the Fermi–Dirac function for the left and right electrodes with the chemical potential $\mu_{L(R)}$.

3 Results and discussion

As mentioned above, the magnetic properties of $Fe(stpy)_4(NCX)_2$ isomers depend on the stpy ligand.[21] The isomer with the *cis* configuration remains in the HS state at all temperature due to the decrease in the ligand field strength, while the *trans*-isomer undergoes a spin crossover process. Here, we try to explore the transport properties of $Fe(stpy)_4(NCS)_2$ SCO complexes with the *trans* and *cis* configurations, and then demonstrate that they hold the promising for molecular spintronic devices.

3.1 *trans* configuration

We start with performing spin-polarized DFT calculations for the geometric, magnetic, electronic, and transport properties of the free $Fe(stpy)_4(NCS)_2$ SCO complex with the *trans* configuration in the first subsection. Fig. 1(a) shows the optimized geometric structures. The relaxed Fe–N bond distances are predicted to be about 2.06 and 2.26 Å along the axial and equatorial ligands for the HS state with the *trans* configurations, respectively, while the corresponding Fe–N distances are reduced to be about 1.94 and 2.00 Å for the LS state. Clearly, these relaxed key geometric parameters (the Fe–N distances for both axial and the equatorial ligands) are capable of reproducing the crystallographic parameters and previous theoretical results.[16,21] The relatively longer Fe–N distances in the pseudo-octahedral coordination lead to the local relatively weak crystal field, corresponding to the HS state. The corresponding magnetic moment is predicted to be about 4.0 μ_B, which mainly come from the central Fe ions. As for the LS state, the ground state of $Fe(stpy)_4(NCS)_2$ SCO magnet with the *trans* configuration is spin-restricted, and the magnetic moment is zero.

Moreover, we find that the electronic structures of $Fe(stpy)_4(NCS)_2$ SCO complex with the *trans* configuration are dramatically different for the HS and LS states. Fig. 1(b) presents their energy positions and the spatial distribution of the Frontier orbitals of two different spin states. It is clear that the energy gap between the highest occupied molecular orbital (HOMO) and lowest unoccupied molecular orbital (LUMO) for the spin-up channel of the HS state is 1.61 eV, which is larger than that of the spin-down channel (0.38 eV), and also larger than the energy gap (0.67 eV) of the LS state. Moreover, all HOMO of the *trans* configuration are mainly delocalized along the axial direction of the stpy ligands, showing the π-type orbital feature, and distribution along the NCS equatorial ligands. On the contrary, the spatial distribution of all LUMO along the NCS equatorial ligands is disappear. These observed remarkable differences in the geometric and electronic

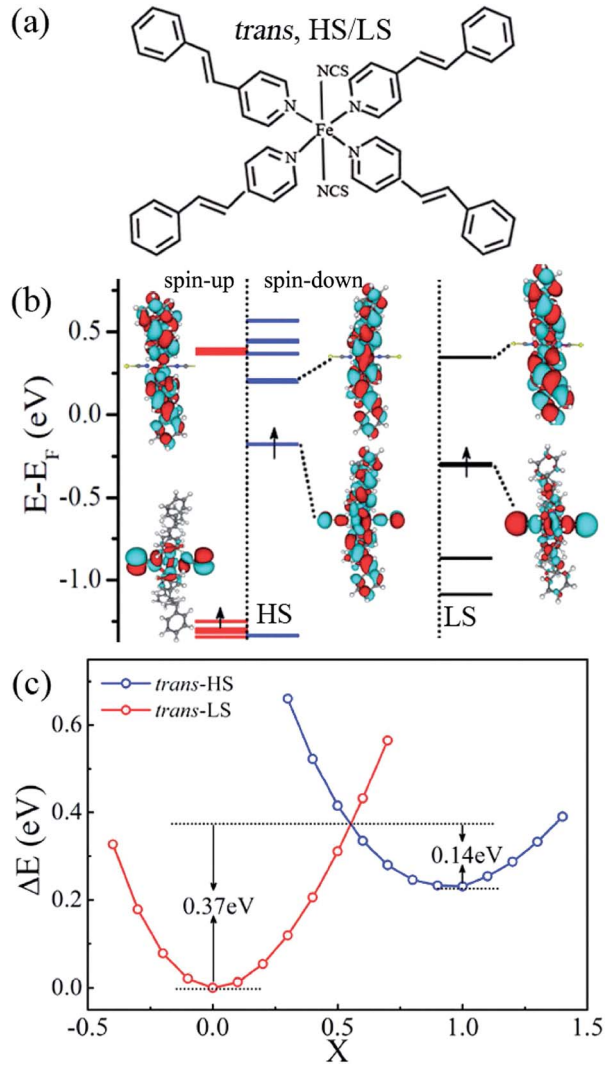

Fig. 1 (a) Schematic diagram of the isolated $Fe(stpy)_4(NCS)_2$ SCO complex for the *trans* configuration. (b) Spatial distribution and the energy level of the Frontier molecular orbitals. (c) The relative total energies of $Fe(stpy)_4(NCS)_2$ SCO complex with the *trans* configuration for the HS and LS states along the reaction coordinates (X).

structures of $Fe(stpy)_4(NCS)_2$ SCO complex with the *trans* configuration for two spin channels suggest that it is a possible candidate for designing molecular spintronic devices.

In experiments, $Fe(stpy)_4(NCS)_2$ complexes with the *trans* configuration undergoes spin crossover around 160 K.[16–18] To estimate the energy barrier of the spin transition between the HS state ($S = 2$) and LS state ($S = 0$), we calculate the total energies of two different spin states as a function of the reaction coordinates (X), which is defined as the interpolation between the LS ($X = 0$) and the HS ($X = 1$) geometries, and the corresponding results are plotted in Fig. 1(c). Clearly, the LS state is predicted to be the ground state as expected, The total electronic energy for the HS state ($X = 1$) is larger about 0.23 eV than that of the LS state ($X = 0$, the ground state), which agrees well with the pervious experimental and theoretical works.[21,30] Test calculations of the Gibbs free energies *via* considering the thermal contribution, we find that the LS state will be more stable about 0.28 eV. These observations indicate that the TPSSh functional is capable of reproducing this examined Fe-based spin-crossover behavior.[30] With the increase of reaction coordinates from $X = 0$, the total energy of the LS state gradually increases. Then there is a cross with the energy curve of the HS state around ~0.55. The energy barrier is about 0.37 eV, which can be overcome by external stimuli, *i.e.* temperature or light.[16–18] It is clear that the spin transition is accompanied by the geometrical structure modifications. In other words, the spin transition can be realized by changing the metal-to-ligand Fe–N bond distances *via* external stimuli. Then the weak and strong crystal fields correspond to $Fe(stpy)_4(NCS)_2$ magnets with the HS and LS states, respectively.

To explore the transport properties of $Fe(stpy)_4(NCS)_2$ complex with the *trans* configuration, the Fe-based SCO complex is sandwiched between two Au(100) nanoelectrodes, as shown in Fig. 2(a). The proposed two-probe junction can be divided into three parts, including the left and right electrodes, and the extended molecule, which contains the sandwiched

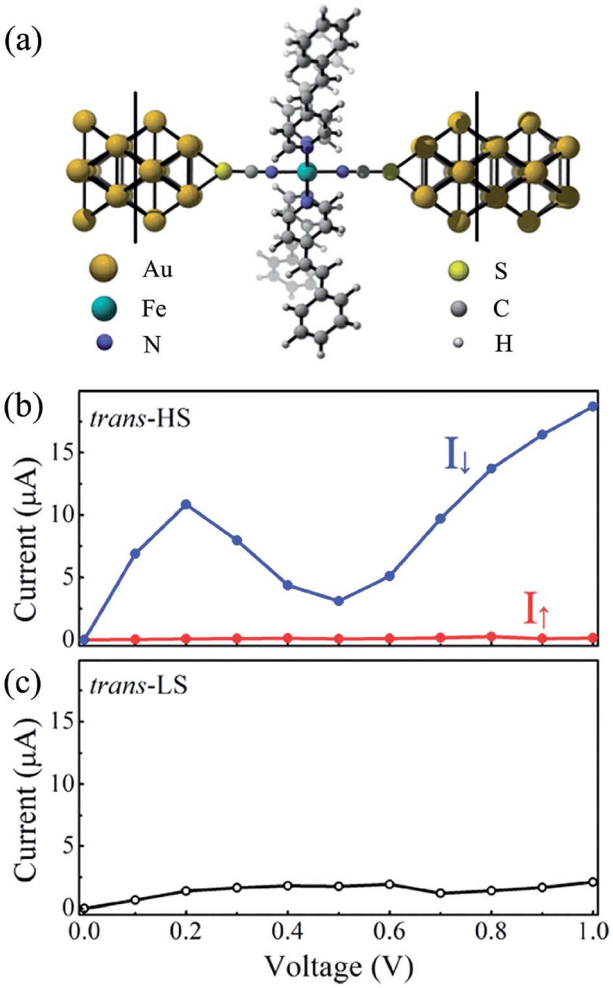

Fig. 2 (a) Schematic illustration of the proposed molecular junction, here, $Fe(stpy)_4(NCS)_2$ complex with the *trans* configuration is sandwiched between two Au(100) nanoelectrodes. (b) The I–V curves through $Fe(stpy)_4(NCS)_2$ junction with the HS state, the red and blue lines stand for the spin-up and spin-down electrons, respectively, (c) the I–V curve for the LS state.

$Fe(stpy)_4(NCS)_2$ complex, two and three surface layers of the left and right electrodes, respectively. Here, the charge distribution in the electrodes present the similar properties as that of the bulk materials due to the screening effects. In our simulations, we fix $Fe(stpy)_4(NCS)_2$ molecular structure obtained at the TPSSh functional level and optimize the anchoring Au–S distance. According to the calculated adsorption energies, we find that this Fe-based SCO complex refers to adsorb on the hollow sites of Au(100) surface. The anchoring Au–S distance is predicted to be about 2.55 Å, which is close to the adopted value in the previous investigations.[31] Note that this kind of anchor type has been commonly adopted in previous reports.[32–34]

Fig. 2(b) and (c) show the calculated current–voltage (*I–V*) curves of $Fe(stpy)_4(NCS)_2$ SCO complexes the HS and LS states. Here, at each bias voltage, the current is determined self-consistently under the non-equilibrium conditions. It is clear that the *I–V* curves for the HS and LS states display the dramatically distinctive properties. The current through the Fe-based SCO complex with the HS state is significantly larger than that of the LS state. For example, the current for the HS and LS states at 0.2 V is predicted to be 10.93 and 1.40 μA, respectively. This observation means that the molecular junction with the LS state can be turned from OFF state to ON state by the LS → HS spin transition. That is to say, this Fe-based SCO complex with the *trans* configuration could act as a molecular switch when the spin transition is triggered by external stimuli, *i.e.* light. Similar transport behavior has also been found for Fe(II)–N_4S_2 SCO complex.[35]

As for $Fe(stpy)_4(NCS)_2$ complex with the HS state, the currents through the spin-up and spin-down electrons are plotted with the red and blue lines, as shown in Fig. 2(b), respectively. Two following interested features are observed:

(i) The *I–V* curves through $Fe(stpy)_4(NCS)_2$ complex with the HS state display a nearly perfect spin-filtering effect. The current of the spin-down electrons ($I_\downarrow$) through Fe-based SCO complex is significantly larger than that of the spin-up electrons ($I_\uparrow$). At the bias voltage of 0.2 V, $I_\uparrow$ and $I_\downarrow$ is about 0.09 and 10.84 μA, respectively. The current difference between two spin channels under different bias voltages can be quantified by the ratio of current defined as $R(V) = I_\downarrow$ and $I_\uparrow$. The calculated R varies from 37 to 170 in the bias range of [0.1, 1.0 V].

(ii) An obvious negative differential resistance (NDR) effect appears for the spin-down channel. With increasing of the bias voltage, the current ($I_\downarrow$) gradually increases, then it reaches to the maximum value of 10.84 μA at 0.2 V. At 0.5 V, the $I_\downarrow$ decreases to the minimum value of 3.11 μA, resulting in a NDR phenomenon. When the bias voltage continuously increases, the current increases almost linearly. This observed NDR effect is similar to that of various molecules sandwiched between two N doped graphene nanoribbons.[36]

Clearly, the switch between the HS and LS states, nearly perfect spin-filtering effect, and obvious NDR behavior observed in $Fe(stpy)_4(NCS)_2$ SCO complex with the *trans* configuration are desirable features with ample applications in future molecular spintronics.

As shown in eqn (2), the current values are determined by integrating the transmission coefficients with a given bias voltage range. To clearly illustrate the transport mechanism of $Fe(stpy)_4(NCS)_2$ SCO complex with the *trans* configuration, we calculate the zero-bias transmission spectra as a function of the energy for both the HS and LS states, and the corresponding results are plotted in Fig. 3(a) and (b), respectively. Here, the Fermi level is set as zero for clarity, and these empty triangles stand for the eigenvalues of the molecular projected self-consistent Hamiltonian (MPSH), which can be referred as perturbed molecular orbitals because of the presence of Au electrodes. Clearly, as for the HS state, the transport properties of $Fe(stpy)_4(NCS)_2$ SCO complex with the *trans* configuration are dominated by the spin-down electron, similar to the previous reported results for Fe_2 complexes and iron-phthalocyanine.[33,37] There are two significant transmission peaks locating at −0.02 eV and 0.36 eV, which is contributed by the perturbed HOMO and LUMO, respectively, since all coefficients of the spin-up electrons are close to zero within the energy range of [−1.0, 1.0 eV]. This result can be used to explain the observed spin-filtering effect, as shown in Fig. 3(b). To quantify the spin filter efficiency (SFE), defined as $|T_\uparrow(E_F) - T_\downarrow(E_F)|/|T_\uparrow(E_F) + T_\downarrow(E_F)|$ in our calculations, where $T_\uparrow(E_F)$ and $T_\downarrow(E_F)$ stand for the transmission coefficient of the spin-up and spin-down channels at the Fermi level, respectively. The calculated $T_\uparrow$ and $T_\downarrow$ through molecular junction at the Fermi level is about 0.009 and 1.89, respectively. The SFE is predicted to be about 99%, nearly perfect spin-filtering effect, for $Fe(stpy)_4(NCS)_2$ SCO complex with the *trans* configuration.

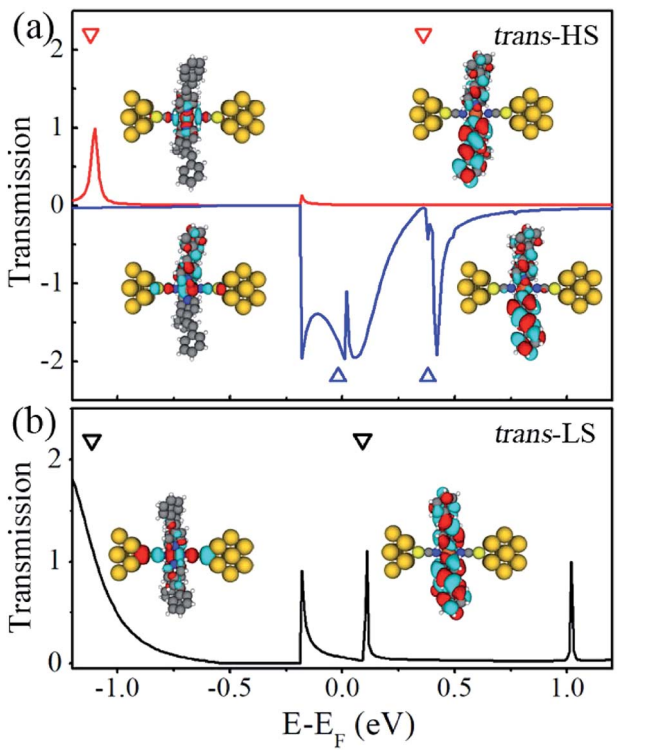

Fig. 3 Zero-bias transmission spectra of $Fe(stpy)_4(NCS)_2$ complex with the *trans* configuration. (a) For the HS state, the red and blue lines stand for spin-up and spin-down electrons, respectively. (b) For the LS state, here, the insets are the spatial distribution of the perturbed HOMO and LUMO.

Actually, the spatial distribution of the perturbed HOMO and LUMO can be used to understand the calculated transmission curves. For example, the perturbed LUMO of the spin-up electrons mainly delocalizes on the plane of stpy ligands, but it almost disappears along the NSC ligands connecting to Au electrodes. This is the reason why there is not a transmission peak, originating from the perturbed LUMO. The significant transmission peak (at −0.02 eV) comes from the perturbed HOMO of $Fe(stpy)_4(NCS)_2$ complex with *trans* configuration due to the delocalization of along the NCS ligands, which benefits for the transport through this Fe-based SCO complex *via* the NCS ligands. Of course, the energy positions of the perturbed MOs relative to the Fermi level match nicely with the transmission peaks for two spin channels. The energy gaps between the perturbed HOMO and LUMO of the spin-up and spin-down electrons are predicted to be 1.48 and 0.40 eV for the HS state, which are close to the results presented in Fig. 1(b).

As for the LS state, the significant transmission peak at −0.19 eV originates from the perturbed HOMO, and the perturbed LUMO contributes the narrow transmission peak locating at 0.11 eV, which results in the small current through $Fe(stpy)_4(NCS)_2$ SCO complex with the *trans* configuration under small bias voltage range.

To further explore the mechanism the observed NDR effect in the *I*–*V* curve of the spin-down electrons ($I_\downarrow$), we plot the spin-polarized transmission spectra at the different bias voltages in Fig. 4, here, the dotted line indicates the integration bias range of the *I*–*V* curve for clarity. It is clear that the position of the transmission peaks near the Fermi level gradually shift and their shapes change dramatically with the applied bias voltage. The broad and large transmission peak coming from the perturbed HOMO, which lies in the integral range, dominates the current ($I_\downarrow$). With increasing of the bias voltage, the current gradually increases, and it reaches to the maximum about 10.84 μA at 0.2 V, when $V < 0.2$ V. When the bias voltage continuously increases, *i.e.* to 0.3 V, this transmission peak splits into two peaks with relative small transmission coefficients, which results in the current reduction in the bias range of [0.2, 0.5 V], and the minimum current is about 3.11 μA at 0.5 V. When the applied bias voltage is larger than 0.5 V, there is a new transmission peak entering into the integral window, the current increases again. Here, we conclude that the bias-dependent transmission are responsible for the observed NDR phenomenon.

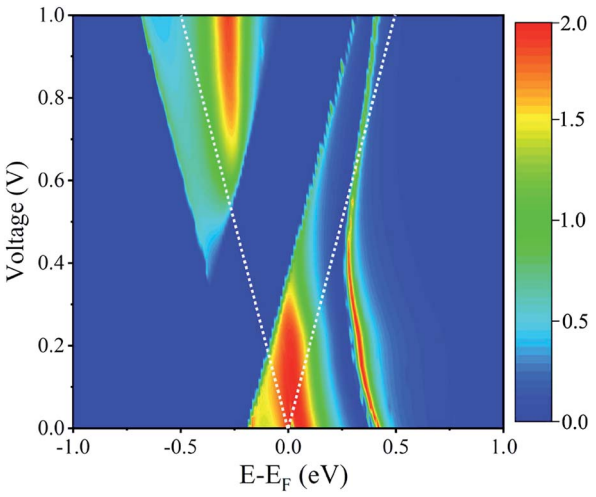

Fig. 4 Bias-dependent transmission spectra for the spin-down electrons of $Fe(stpy)_4(NCS)_2$ SCO complex with the HS state.

3.2 *cis* configuration

Now we focus on $Fe(stpy)_4(NCS)_2$ SCO complex with the *cis* configuration, as shown in Fig. 5(a), in which all stpy ligands present the *cis* configuration. The relaxed Fe–N distances are predicted to be about 2.02 and 2.30 Å for the axial and equatorial directions, respectively. The relative long Fe–N bond lengths lead to the weak crystal field, which accounts for the observed HS state for $Fe(stpy)_4(NCS)_2$ SCO complex with the *cis* configuration in experiment.[16] The molecular magnetic moments is about 4.0 μ_B, while the Fe atomic magnetic moment is about 4.2 μ_B. Although only the HS state is observed for the *cis* configuration in experiment, we suggest that the spin transition between the *cis*-HS and *trans*-LS states is possible *via* the *cis*–*trans* isomerization, similar to the previous investigation of Boillot *et al.*[17] Fig. 5(b) plots the calculated total energies as a function of the reaction coordinates (*X*), defined as the interpolation between the *trans*-LS ($X = 0$) and *cis*-HS ($X = 1$) configurations. It is clear that the total energy of the *cis*-HS

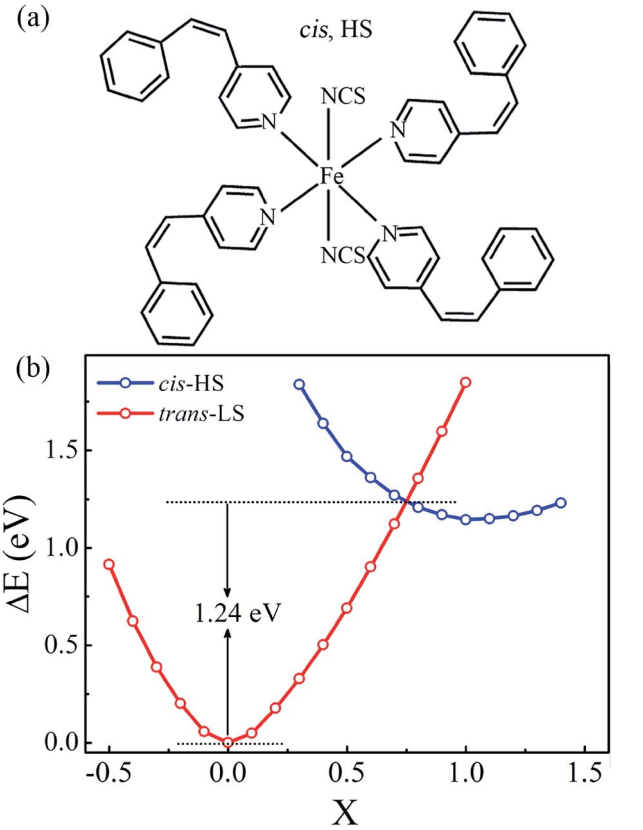

Fig. 5 (a) Schematic diagram of $Fe(stpy)_4(NCS)_2$ SCO complex with the *cis* configuration, (b) the relative total energies of $Fe(stpy)_4(NCS)_2$ SCO complexes with the *cis*-HS and *trans*-LS configurations along the reaction coordinates (*X*).

configuration is larger than that of the *trans*-LS configuration of 1.14 eV. The spin transition occurs at $X \sim 0.75$, and the corresponding transition barriers is predicted to be about 1.24 eV, implying that the photoisomerization between the *trans* and *cis* configurations maybe realized under visible light radiation in $Fe(stpy)_4(NCS)_2$ SCO complex with the *cis* configuration.

Fig. 6(a) illustrates the proposed $Fe(stpy)_4(NCS)_2$ SCO molecular junction with the *cis* configuration. The calculated *I*–*V* curves and spin-polarized transmission spectra the *cis*-HS state are plotted in Fig. 6(b) and (c), respectively. It is clear that the obtained transport properties through the *cis*-HS configuration are similar to that of $Fe(stpy)_4(NCS)_2$ SCO complex with the *trans*-HS configuration. The delocalization of the perturbed HOMO along the NCS ligands connecting to electrodes provides a good conducting channel, as shown the inserts in Fig. 6(c). The conductance of $Fe(stpy)_4(NCS)_2$ SCO complex with the *cis* configuration is mainly dominated by the spin-down electrons due to the large and broad transmission peak locating around the Fermi level, which is contributed by the perturbed HOMO. The current of the spin-up electrons is less than that of the spin-down electrons. Nearly perfect spin-filtering effect and obvious NDR behavior are observed again in $Fe(stpy)_4(NCS)_2$ SCO complex with the *cis*-HS configuration, implying that this Fe-based SCO complex with the *cis* configuration can be also used to design molecular devices.

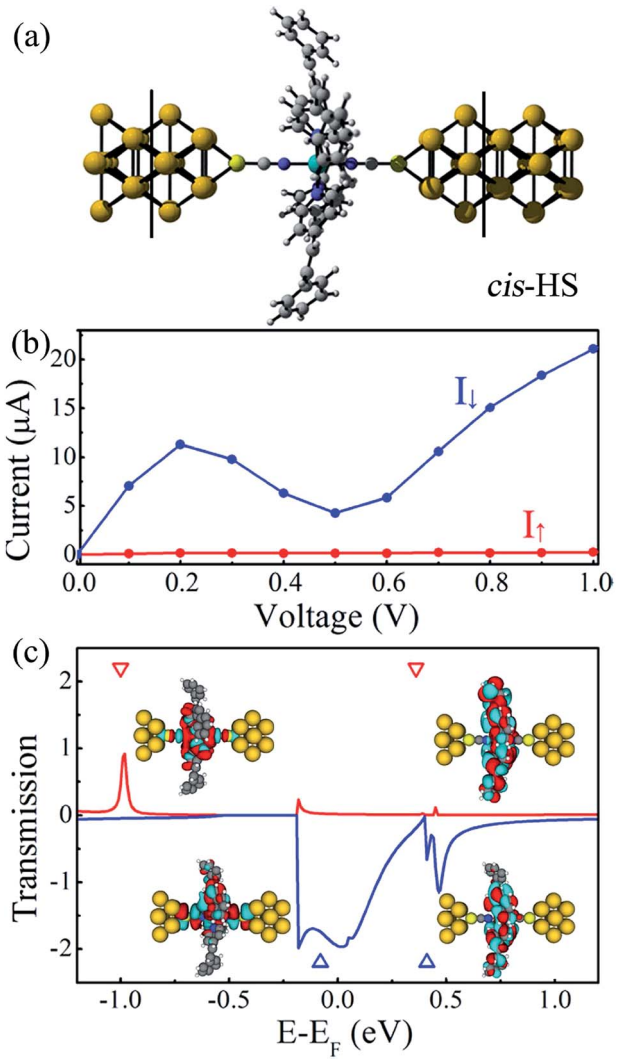

Fig. 6 (a) Schematic illustration of the proposed junction, $Fe(stpy)_4(NCS)_2$ with the *cis*-stpy isomer is sandwiched between two Au(100) electrodes. (b) The *I*–*V* curves of $Fe(stpy)_4(NCS)_2$ junctions with the *cis* configuration. (c) Zero-bias transmission spectra as a function of the energy, here, the red and blue lines corresponded with the spin-up and spin-down channels, while the inserts stands for the spatial distribution of the perturbed HOMO and LUMO.

Finally, we perform additional transport calculations using the DFT+U (*U* is set to be 4.3 eV) method to check reliability of above presented results obtained at the GGA-PBE level. Fortunately, the DFT+U calculations qualitatively do not change the results given by the PBE functional. The position and shape of the transmission peaks just change slightly within [−0.5, 0.5 eV] energy window.

4 Conclusions

In summary, based on density functional theory calculations combined with non-equilibrium Green's function method, we explore the transport behaviors of $Fe(stpy)_4(NCS)_2$ LD-LISC SCO complexes with the *trans* and *cis* configurations. The calculated transport results clearly reveal that the current through the molecular junction with the HS state is significantly larger than that of the LS state, which indicates that this Fe-based LD-LISC SCO complex with the *trans* configuration could act as a molecular switch when the spin transition is triggered by external stimuli. Due to the remarkably different electronic structures of two spin channels and the bias-dependent transmission spectra, we observe the nearly perfect spin-filtering effect and obvious negative differential resistance feature in this examined $Fe(stpy)_4(NCX)_2$ with the *trans* and *cis* configurations. Moreover, the predicted energy barrier between the *cis*-HS and *trans*-LS states of this Fe-based LD-LISC SCO magnets is about 1.24 eV, implying that it is possible to realize the SCO phenomena under the visible light radiation in experiments. Clearly, these presented theoretical results imply that the examined Fe-based LD-LISC SCO complexes are promising building blocks in molecular spintronic functional devices.

Conflicts of interest

There are no conflicts to declare.

Acknowledgements

This work was partially supported by National Key Research & Development Program of China (No. 2016YFA0200600), the National Natural Science Foundation of China (No. 21873088 and 11634011), and the Natural Science Foundation of the Anhui Higher Education Institutions (No. KJ2010A061 and KJ2016A144). Computational resources have been provided by CAS, Shanghai and USTC Supercomputer Centers.

References

1 A. Bousseksou, G. Molnár, L. Salmon and W. Nicolazzi, *Chem. Soc. Rev.*, 2011, **40**, 3313.

2 P. Gütlich, *Eur. J. Inorg. Chem.*, 2013, **5–6**, 581.
3 K. S. Kumar and M. Ruben, *Coord. Chem. Rev.*, 2017, **346**, 176.
4 G. Molnár, S. Rat, L. Salmon, W. Nicolazzi and A. Bousseksou, *Adv. Mater.*, 2017, **30**, 17003862.
5 P. Gütlich, A. B. Gaspar and Y. Garcia, *Beilstein J. Org. Chem.*, 2013, **9**, 342.
6 H. Phan, J. Hrudka, D. Igimbayeva, L. M. L. Daku and M. Shatruk, *J. Am. Chem. Soc.*, 2017, **139**, 6437.
7 E. Coronado, J. R. Galán-Mascarós, M. Monrabal-Capilla, J. García-Martínez and P. Pardo-Ibáñez, *Adv. Mater.*, 2007, **19**, 1359.
8 I. Šalitroš, N. T. Madhu, R. Boča, J. Pavlik and M. Ruben, *Monatsh. Chem.*, 2009, **140**, 695.
9 B. Rösner, M. Milek, A. Witt, B. Gobaut, P. Torelli, R. H. Fink and M. M. Khusniyarov, *Angew. Chem., Int. Ed.*, 2015, **54**, 12976.
10 M. M. Khusniyarov, *Chem.–Eur. J.*, 2016, **22**, 15178.
11 B. Brachňaková and I. Šalitroš, *Chem. Pap.*, 2018, **72**, 773.
12 D. H. Waldeck, *Chem. Rev.*, 1991, **91**, 415.
13 T. Shen, X. N. Wang and H. X. Lou, *Nat. Prod. Rep.*, 2009, **26**, 916.
14 M. Milek, F. W. Heinemann and M. M. Khusniyarov, *Inorg. Chem.*, 2013, **52**, 11585.
15 M. Dommaschk, M. Peters, F. Gutzeit, C. Schütt, C. Näther, F. D. Sönnichsen, S. Tiwari, C. Riedel, S. Boretius and R. Herges, *J. Am. Chem. Soc.*, 2015, **137**, 7552.
16 C. Roux, J. Zarembowitch, B. Gallois, T. Granier and R. Claude, *Inorg. Chem.*, 1994, **33**, 2273.
17 M. L. Boillot, J. Zarembowitch and A. Sour, *Top. Curr. Chem.*, 2004, **234**, 261.
18 M. L. Boillot, S. Pillet, A. Tissot, E. Rivière, N. Claiser and C. Lecomte, *Inorg. Chem.*, 2009, **48**, 4729.
19 A. Tissot, M. L. Boillot, S. Pillet, E. Codjovi, K. Boukheddaden and L. M. L. Daku, *J. Phys. Chem. C*, 2010, **114**, 21715.
20 A. Sugahara, K. Moriya, M. Enomoto, A. Okazawa and N. Kojima, *Polyhedron*, 2011, **30**, 3127.
21 J. Cirera and F. Paesani, *Inorg. Chem.*, 2012, **51**, 8194.
22 C. Lefter, V. Davesne, L. Salmon, G. Molnár, P. Demont, A. Rotaru and A. Bousseksou, *Magnetochemistry*, 2016, **2**, 18.
23 N. Gallego-Planas, A. Martín-Rodríguez and E. Ruiz, *Dalton Trans.*, 2016, **45**, 18867.
24 M. J. Frisch, G. W. Trucks and H. B. Schlegel, *et al.*, *Gaussian 09*, Wallingford, CT, 2009.
25 A. Schäfer, C. Huber and R. Ahlrichs, *J. Chem. Phys.*, 1994, **100**, 5829.
26 J. Cirera and E. Ruiz, *J. Mater. Chem. C*, 2015, **3**, 7954.
27 K. P. Keep, *Inorg. Chem.*, 2016, **55**, 2717.
28 J. Taylor, H. Guo and J. Wang, *Phys. Rev. B: Condens. Matter Mater. Phys.*, 2001, **63**, 245407.
29 M. Brandbyge, J. L. Mozos, P. Ordejón, J. Taylor and K. Stokbro, *Phys. Rev. B*, 2002, **65**, 165401.
30 H. Paulsen, V. Schünemann and J. A. Wolny, *Eur. J. Inorg. Chem.*, 2013, **46**, 628.
31 M. D. Ventra, S. T. Pantelides and N. D. Lang, *Phys. Rev. Lett.*, 2000, **84**, 979.
32 D. Aravena and E. Ruiz, *J. Am. Chem. Soc.*, 2012, **134**, 777.
33 J. Huang, R. Xie, W. Y. Wang, Q. X. Li and J. L. Yang, *Nanoscale*, 2016, **9**, 609.
34 A. Martín-Rodríguez, D. Aravena and E. Ruiz, *Theor. Chem. Acc.*, 2016, **135**, 192.
35 M. L. Du, Y. J. Hu, J. Huang and Q. X. Li, *Chin. J. Chem. Phys.*, 2018, **31**, 33.
36 J. Huang, W. Y. Wang, Q. X. Li and J. L. Yang, *J. Chem. Phys.*, 2014, **140**, 164703.
37 J. Huang, K. Xu, S. L. Lei, H. B. Su, S. F. Yang, Q. X. Li and J. L. Yang, *J. Chem. Phys.*, 2012, **136**, 064707.